THESIS FOR THE DEGREE OF DOCTOR OF PHILOSOPHY IN SOLID AND
STRUCTURAL MECHANICS

On Computational Homogenization of Fluid-filled Porous Materials

CARL SANDSTRÖM

On Computational Homogenization of Fluid-filled Porous Materials

CARL SANDSTRÖM
ISBN 978-91-7597-162-9

Cover:
Fluid and solid phase in a Representative Volume Element under shear deformation and a prescribed hydrostatic pressure in the fluid. The image to the left shows the velocity field of the deformed fluid domain and the image on the right shows the von Mises stress of the deformed solid.

On Computational Homogenization of Fluid-filled Porous Materials

Thesis for the degree of Doctor of Philosophy in Solid and Structural Mechanics
CARL SANDSTRÖM
Department of Applied Mechanics
Chalmers University of Technology

Abstract

Porous materials are present in many natural as well as engineered structures. Engineering examples include filters, sanitary products and foams while examples of natural occurrences are oil reservoirs and biological tissue. These materials possess a strongly heterogeneous microstructure consisting of a contiguous solid skeleton, more or less saturated with fluid. The scale of the substructural features is normally much smaller than that of the engineering structure. For instance, groundwater flow takes place at a length scale of kilometers while the pores and channels where the fluid is transported have a length scale of millimeters. Thus, taking the complete microstructure into consideration when performing analysis on such structures is simply too computationally demanding.

Traditionally, computations on porous materials are performed using phenomenological models, the simplest one being the linear Darcy's law which relates the seepage and pressure gradient. However, this thesis concerns the modeling of porous materials using homogenization, where the macroscale properties are derived from the subscale. This technique can either be used to calibrate existing phenomenological models or in a fully concurrent setting where a subscale model replaces the macroscale material model in each Gauss point in an FE-setting. The latter constitutes the so-called FE^2-approach. The obvious drawback of FE^2 is that the computational cost, while smaller than the fully resolved case, is still high. Due to its mathematical and physical consistency, the method used is the Variationally Consistent Homogenization method.

The ultimate goal of this work is to predict the mechanical behaviour of a two-phase material consisting of fluid that flows through a deformable open-pore solid. An important feature is that interaction between the solid and the fluid phases is taken into account. It is required that the modeling is performed in 3D, since the solid phase in a 2D model of a porous material is not connected and can, therefore, not sustain mechanical loading. The issue of imposing periodic boundary conditions on a unstructured, non-periodic mesh is addressed. Numerical results include the assesment of how the pore characteristics affect the macroscopic permeability, comparison of solutions pertaining to the fully resolved problem versus the homogenized problem, performance of weakly periodic boundary conditions and the interaction of fluid and deforming solid.

Keywords: porous materials, homogenization, multiscale modeling, Stokes flow, Darcy flow

To Charlie, Sixten and the one in Michaelas tummy.

Preface

The work presented in this thesis was carried out at the Division of Material and Computational Mechanics at Chalmers University of Technology during 2009-2015. The research was funded by Swedish Research Counsel (Vetenskapsrådet).

First, I would like to thank my main supervisor Professor Fredrik "the Mathemagician" Larsson for his guidance during this time. I would also like to thank my co-supervisors, Professor Kenneth "Red-pen" Runesson and Doctor Håkan Johansson, for their help and valuable input. Moreover, I would like to thank all my colleagues at the third floor for creating such a nice working environment.

Finally, I would like to thank my family, Michaela and Sixten, for their love, support and, foremost, their patience.

Thesis

This thesis consists of an extended summary and the following appended papers:

Paper A
C. Sandström and F. Larsson. Variationally Consistent Homogenization of Stokes Flow in Porous Media. *International Journal for Multiscale Computational Engineering* **11**.2 (2013), 117–138. ISSN: 1543-1649. DOI: 10.1615/IntJMultCompEng.2012004069. URL: http://www.begellhouse.com/journals/61fd1b191cf7e96f,6218a4594d64a04c,4e77728141fddda9.html

Paper B
C. Sandström, F. Larsson, K. Runesson, and H. Johansson. A Two-scale Finite Element Formulation of Stokes Flow in Porous Media. *Computer Methods in Applied Mechanics and Engineering* **261-262** (July 2013), 96–104. ISSN: 00457825. DOI: 10.1016/j.cma.2013.03.025. URL: http://linkinghub.elsevier.com/retrieve/pii/S0045782513000856

Paper C
C. Sandström, F. Larsson, and K. Runesson. Weakly Periodic Boundary Conditions for the Homogenization of Flow in Porous Media. *Advanced Modeling and Simulation in Engineering Sciences* **1**.1 (2014), 12. ISSN: 2213-7467. DOI: 10.1186/s40323-014-0012-6. URL: http://www.amses-journal.com/content/1/1/12

Paper D
C. Sandström and F. Larsson. On Bounded Approximations of Periodicity for Computational Homogenization of Stokes Flow in Porous Media. *Submitted for international publication* ()

Paper E
C. Sandström, F. Larsson, and K. Runesson. Homogenization of Coupled Flow and Deformation in a Porous Material. *To be submitted* ()

All papers were prepared in collaboration with the co-authors. The author of this thesis was responsible for the major progress of the work in preparing the papers, i.e. took part in planning the papers, took part in developing the theory, developed numerical implementations and carried out the numerical simulations.

CONTENTS

Part I

Extended Summary

1 Introduction

In general, most material makes the impression to consist of one single constituent. Yet, if we zoom in sufficiently on the material, its heterogeneous microstructure is revealed. For instance, steel consists of very small crystals in various orientations. Due to the great difference in scales, the behavior of the material appears to be homogeneous on the macroscale. However, it is in fact the microstructural geometry and the material composition that determine the macroscopic behavior.

Porous media constitute a class of materials with a microstructure consisting of at least two phases: the solid skeleton and one (or more) fluids. This class is of great importance in many engineering fields such as geology and biomechancis. Examples are rock, bone tissue, wood and foams. Engineering applications range from CO_2 storage to filters and insulation materials. Images of three different microstructures are shown in Figure 1.1. The microstructures of glass fiber, human bone and clay (Figures 1.1(a), 1.1(b) and 1.1(d), cf. refs [8], [38] and [37]) are of random type while that of polyurethan foam (Figure 1.1(c), cf. ref [7]) exhibits a periodic microstructure.

| (a) | (b) | (c) | (d) |
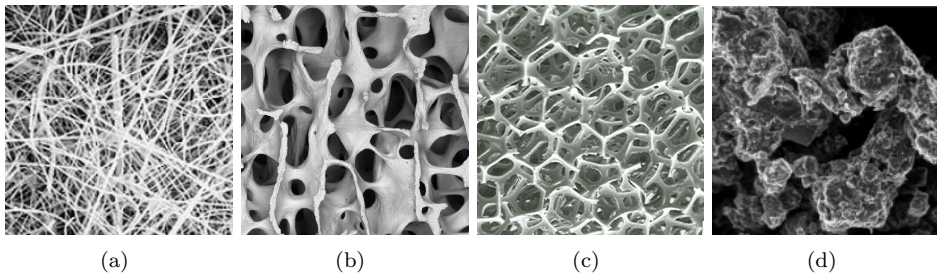
Figure 1.1: Microstructure of (a) Glass fiber (b) Human bone (c) Polyurethan foam (d) Clay

A wide range of material characteristics can be found in porous media. For instance, the solid phase can be of contiguous nature, such as a sponge, or consist of discrete particles, such as sand. The pore system can be open, whereby the pores are connected, or closed, whereby no channels between pores are present. Naturally, for a fluid to be able to flow through the material, it has to be of open-pore type.

Indeed, the difference in length scales of the application and the microstructure can be very large. For example, groundwater flow can be at a length scale of kilometers while

the pore space in which the fluid is transported is at a length scale of millimeters.

The traditional approach is to establish phenomenological models, whereby the difficulties involved in taking the microstructure into account are avoided. Numerical values of the models parameters are determined experimentally via, more or less standard, inverse analysis. An obvious advantage of phenomenological models is that they are computationally efficient. However, as they are calibrated from experimental results they are less flexible when it comes to representing the intrinsic physical properties. For instance, a change of material composition, say from water to oil, calls for new experimental results and possibly the use of another material model.

A more fundamental approach to modeling is to take the microstructural properties into account through homogenization, whereby we choose to mimic a small piece of material in what is known as a Representative Volume Element (RVE). This technique can be used to either calibrate existing macroscopic phenomenological models, so-called upscaling, or in a concurrent multiscale setting (FE^2), where the RVE problem is solved in each macroscale point. The RVE contains a geometric representation of the microstructure along with solid and fluid material data. By imposing suitable conditions on the fields within the RVE, we can compute the macroscopic response of the substructure.

2 Aim of research

The main objective of this work is to establish a model framework, based on homogenization, that is capable of capturing the complex behavior of a porous material, where a fluid is contained within a deformable solid skeleton with an open pore system. The model should be able to predict the response of the porous material in terms of pressure, pressure gradient and deformation fields. In particular, to allow for deformations in a porous material, the modeling has to be conducted in 3D. In order to achieve the stated goal, the following subtasks are identified:

- Establish a theoretical framework for homogenization that relies on the concept of variational consistency.

- Resolve issues concerning how to impose periodic boundary conditions on the RVE for the pertinent multifield problem.

- Develop and incorporate a model based on subscale Fluid-Structure-Interaction (FSI) in the theoretical framework for homogenization.

- Implement numerical algorithms in a suitable FE-software.

3   Subscale model - Fully resolved problem

3.1   Preliminaries

Since the deformation of the solid and the motion of the contained fluid is coupled, such that the flow changes the geometry of the solid which, in turn, changes the geometry of the fluid domain, a relevant subject is that of FSI [12]. There are primarily two approaches to FSI; the monolithic and the staggered approach. In the monolithic approach, the equations of the solid and fluid phases are solved simultaneously. In the staggered approach, on the other hand, the equations for each phase are solved in an iterative manner until convergence is reached. Monolithic solvers are more robust as compared to staggered solvers, while the latter are less expensive in terms of computational cost. A comparison of the two approaches is found in [10].

3.2   Decoupled problem

In this thesis, we study the quasi-static incompressible flow in the low Reynolds numbers regime. This assumption is justified when the pores are small cf. [16]. We assume that only two-phases are present: a solid and a fluid. The fluid is contained within a solid skeleton that may be deformable or (in the extreme) can be considered rigid.

As a first step, we consider the case where the fluid-structure coupling is weak. This situation is at hand when the solid is stiff enough not to be significantly deformed (i.e. we employ small deformation theory). Hence, we only consider one-way coupling which corresponds to making one single iteration in the staggered approach. In other words, we compute the flow and the reaction forces on the boundary between the solid and the fluid phases, which may then be applied to the solid.
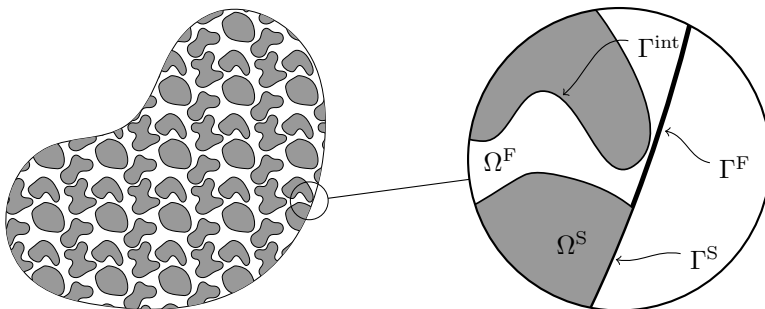

Figure 3.1: Fully resolved domain with magnification of a small part of the boundary and pertinent symbols

Due to the given assumptions, the model for the fluid flow is the Stokes' problem given as

$$-\boldsymbol{\sigma}^{\mathrm{V}} \cdot \boldsymbol{\nabla} + p\boldsymbol{I} = \boldsymbol{0} \qquad \text{in } \Omega^{\mathrm{F}} \tag{3.1a}$$

$$\boldsymbol{v} \cdot \boldsymbol{\nabla} = 0 \qquad \text{in } \Omega^{\mathrm{F}} \tag{3.1b}$$

$$\boldsymbol{v} = \boldsymbol{0} \qquad \text{on } \Gamma^{\mathrm{int}} \tag{3.1c}$$

where $\boldsymbol{\sigma}^{\mathrm{V}} = \boldsymbol{\sigma}^{\mathrm{V}}(\boldsymbol{v} \otimes \boldsymbol{\nabla})$ is the viscous (deviatoric) part of the fluid stress, $\boldsymbol{v}$ is the fluid velocity, p is the hydrostatic pressure, Ω^{F} is the part of Ω containing the fluid phase, and Γ^{int} is the part of $\partial\Omega^{\mathrm{F}}$ that separates the solid and fluid phases, as depicted in Figure 3.1. Equation 3.1c is the no-slip condition which gives rise to stresses in the solid phase due to reaction forces. In order to close the problem, we also introduce Dirichlet boundary conditions, $\boldsymbol{v} = \hat{\boldsymbol{v}}$, and Neumann boundary conditions $\boldsymbol{t}^{\mathrm{F}} = \boldsymbol{\sigma}^{\mathrm{F}} \cdot \boldsymbol{n}^{\mathrm{F}} = \hat{\boldsymbol{t}}$.

In order to compute deformation and stresses in the solid phase, we add the balance equation for the solid phase, i.e.

$$-\boldsymbol{\sigma}^{\mathrm{S}} \cdot \boldsymbol{\nabla} = \boldsymbol{0} \qquad \text{in } \Omega^{\mathrm{S}} \tag{3.2}$$

where $\boldsymbol{\sigma}^{\mathrm{S}}$ is the stress in the solid and Ω^{S} is the solid part of the domain. Assuming (for simplicity) elastic properties of the solid material, we have $\boldsymbol{\sigma}^{\mathrm{S}} = \boldsymbol{\sigma}^{\mathrm{S}}(\boldsymbol{u} \otimes \boldsymbol{\nabla})$ and the pertinent Dirichlet conditions, $\boldsymbol{u} = \hat{\boldsymbol{u}}$, and Neumann conditions $\boldsymbol{t}^{\mathrm{S}} = \boldsymbol{\sigma}^{\mathrm{S}} \cdot \boldsymbol{n}^{\mathrm{S}} = \hat{\boldsymbol{t}}$. In order for Equations 3.1 and 3.2 to describe the coupled behavior of the porous material, we impose the condition pertinent to force equilibrium as

$$\boldsymbol{t}^{\mathrm{S}} + \boldsymbol{t}^{\mathrm{F}} = 0 \qquad \text{on } \Gamma^{\mathrm{int}} \tag{3.3a}$$

where $\boldsymbol{t}^{\mathrm{F}}$ is the (now known) reaction force due to the no-slip condition, i.e. the traction computed as part of the fluid problem in Equation 3.1.

In the appended Papers A to D, the solid phase is considered rigid, thus, the resulting deformation on the solid is not taken into account.

3.3 Fully coupled problem

When the solid phase is soft enough to be deformed by the flow, the strong coupling between the two phases must be taken into account in order to produce reliable computational results. In other words, the deformation imposed on the solid is sufficiently large to alter the fluid domain and, therefore, alter the flow, which in turn alters the deformation of the solid and so on. Naturally, as the deformations are considered large, we employ finite strain theory. Here, we can choose to use either the monolithic or the staggered approach discussed in Section 3.1.

An important difference as compared to the weak coupling is that the no-slip condition now needs to take the motion of the solid into account. Therefore, the condition is given

as

$$\boldsymbol{v} - \mathrm{d}_t \boldsymbol{u} = \boldsymbol{0} \text{ on } \Gamma^{\text{int}} \tag{3.4}$$

where $\boldsymbol{v}$ is the absolute velocity of a fluid particle, $\boldsymbol{u}$ is the displacement of a solid particle and $\mathrm{d}_t \boldsymbol{u}$ is the velocity if the solid. Here, we also note that the boundary Γ^{int} moves as a result of the tractions acting on the solid domain due to the interaction of solid and fluid.

Iliev et al. [14] investigated the application of FSI on the upscaling of properties in porous materials for both small and finite strains. They found that the result correlates well with the solution obtained from Asymptotic Homogenization [29].

Some problems are ill-suited for homogenization, and a fully resolved model is therefore necessary. This applies typically to problems that violate the Separation of Scales condition, e.g. [26], [35]. Naturally, for sufficiently small macroscopic domains, the task of solving the fully resolved problem is not a significant obstacle.

The fully coupled FSI-problem is studied in Paper E in the framework of a monolithic solver.

4 Phenomenological macroscale models

The well-known Darcy's law [6] gives the relation between the pressure gradient and seepage velocity in a porous material. Darcy's law is given as

$$\boldsymbol{w} = -\boldsymbol{K} \cdot \boldsymbol{\nabla} p \tag{4.1}$$

where $\boldsymbol{w}$ is the seepage velocity, $\boldsymbol{K}$ is the permeability of the material, p is the pore pressure and $\boldsymbol{\nabla} p$ is the pressure gradient. The classical definition of $\boldsymbol{w}$ is the rate of fluid volume flowing through a unit area of bulk material.

According to Biot cf. [3], [1], the stress $\boldsymbol{\sigma}$ in a saturated, linearly elastic, porous material, is given as

$$\boldsymbol{\sigma} = \boldsymbol{E} : \boldsymbol{\varepsilon} - \alpha p \boldsymbol{I} \tag{4.2}$$

Hence, the stress is divided into two parts; the solid stress, $\boldsymbol{E} : \boldsymbol{\varepsilon}$, and the intrinsic fluid pressure in the fluid, p. The so-called Biot coefficient α measures how the fluid pressure propagates into the solid.

In summary, for a macroscale model capable of capturing the FSI phenomenon (such as described in Equations 3.1 to 3.3), we have typically the coupled pair of balance equations

$$-\boldsymbol{\sigma} \cdot \boldsymbol{\nabla} = \boldsymbol{0} \tag{4.3a}$$

$$\mathrm{d}_t \Phi + \boldsymbol{\nabla} \cdot \boldsymbol{w} = 0 \tag{4.3b}$$

where Φ is a storage term due to the change in pore space during deformation. Here, three constitutive models are present: the stress $\boldsymbol{\sigma} = \boldsymbol{\sigma}(\boldsymbol{\varepsilon}, p)$, the seepage $\boldsymbol{w} = \boldsymbol{w}(\boldsymbol{\nabla}p)$ and the storage $\Phi = \Phi(\boldsymbol{\varepsilon}, p)$. Typical constitutive models for $\boldsymbol{\sigma}$ and $\boldsymbol{w}$ are given in Equations 4.1 and 4.2. Assuming an elastic, reversible, solid constituent and an incompressible fluid, a linear model is obtained as

$$\Phi = \phi + \alpha\boldsymbol{\varepsilon} : \boldsymbol{I} + \frac{\alpha - \phi}{K^{\mathrm{S}}}p \tag{4.4}$$

where ϕ is the porosity and K^{S} is the intrinsic bulk modulus of the solid material phase. Finally, we note that a dynamic representation of Equation 4.3 is relevant to rapid loading and wave propagation, cf. [22] [2].

5 Variationally Consistent Homogenization

5.1 A model problem

The intent of this section is to briefly review the various steps leading to "Variationally Consistent Homogenization". In order to focus on the essential features, without obscuring the picture with unnecessary modelling complexity, we shall, in the following, consider the Poisson equation with homogeneous boundary conditions as a model problem. The strong form of this problem reads

$$\boldsymbol{\nabla} \cdot \boldsymbol{q} = f \qquad\qquad \text{on } \Omega \tag{5.1a}$$
$$u = 0 \qquad\qquad \text{on } \Gamma \tag{5.1b}$$

where $\boldsymbol{q} = -\boldsymbol{A} \cdot \boldsymbol{\nabla}u$ is the flux (for example, seepage or heat flux), f is a known source, Ω is the computational domain and $\Gamma = \partial\Omega$ is its boundary. Furthermore, $\boldsymbol{A} = \boldsymbol{A}(\boldsymbol{x})$ is a second order tensor which contains material data, e.g. conductivity or permeability, and is assumed to be rapidly fluctuating.

Upon introducing the solution space $\mathcal{U} = \{u : \Omega \to \mathbb{R}, u \text{ suff. regular}, u = 0 \text{ on } \Gamma\}$, we may formulate the weak form in a standard fashion as: Find $u \in \mathcal{U}$ such that

$$a(u, \delta u) = (f, \delta u) \qquad\qquad \forall \delta u \in \mathcal{U} \tag{5.2}$$

where the forms $a(u, \delta u)$ and $(f, \delta u)$ are given as

$$a(u, \delta u) = \int_{\Omega} (\boldsymbol{A} \cdot \boldsymbol{\nabla}u) \cdot \boldsymbol{\nabla}\delta u \,\mathrm{d}V \tag{5.3a}$$

$$(f, \delta u) = \int_{\Gamma} f \delta u \,\mathrm{d}S \tag{5.3b}$$

In the present case, it is also possible to establish a variational format for the fine-scale

6

problem above. Upon introducing the potential energy

$$\Pi\left(\hat{u}\right) \overset{\text{def}}{=} \frac{1}{2}a\left(\hat{u}, \hat{u}\right) - \left(f, \hat{u}\right) \tag{5.4}$$

we note that the solution u of Equation 5.2 is also the minimizer of $\Pi\left(\hat{u}\right)$ on $\mathcal{U}$, i.e.

$$u = \arg\min_{\hat{u} \in \mathcal{U}} \Pi\left(\hat{u}\right) \tag{5.5}$$

and the corresponding stationarity condition becomes

$$\Pi'\left(u; \delta u\right) = a\left(u, \delta u\right) - f(\delta u) = 0 \qquad \forall \delta u \in \mathcal{U} \tag{5.6}$$

which is precisely Equation 5.2.

5.2   Variational Multiscale Method

The Variational Multiscale Method (VMS) was originally introduced by Hughes [13] in the context of the stabilizing the Galerkin method. A non-exhaustive list of problems that can be stabilized using VMS can be found in Brezzi et al. [4]. The main idea is to split the unknown function into a "coarse" (smooth, slowly varying) part and a "fine" (non-smooth rapidly fluctuating) part. This is achieved via the unique hierarchical decomposition $\mathcal{U} = \mathcal{U}^{\text{M}} \oplus \mathcal{U}^{\text{S}}$, such that $u \in \mathcal{U}$ can be uniquely split as $u = u^{\text{M}} + u^{\text{S}}$ with $u^{\text{M}} \in \mathcal{U}^{\text{M}}$ and $u^{\text{S}} \in \mathcal{U}^{\text{S}}$. To avoid technical difficulties, it may be assumed that $u^{\text{S}} = 0$ on Γ for any $u^{\text{S}} \in \mathcal{U}^{\text{S}}$ (such that the boundary data is smooth). In the classical version of VMS, u^{M} is simply taken as the coarse scale FE-solution, $u^{\text{M}} = u_h^{\text{M}}$, on the coarse scale mesh.

Equation 5.2 can now be partitioned as follows: Find $(u^{\text{M}}, u^{\text{S}}) \in \mathcal{U}^{\text{M}} \times \mathcal{U}^{\text{S}}$ such that

$$a\left(u^{\text{M}}, \delta u^{\text{M}}\right) + a\left(u^{\text{S}}, \delta u^{\text{M}}\right) = (f, \delta u^{\text{M}}) \qquad \forall \delta u^{\text{M}} \in \mathcal{U}^{\text{M}} \tag{5.7a}$$
$$a\left(u^{\text{M}}, \delta u^{\text{S}}\right) + a\left(u^{\text{S}}, \delta u^{\text{S}}\right) = (f, \delta u^{\text{S}}) \qquad \forall \delta u^{\text{S}} \in \mathcal{U}^{\text{S}} \tag{5.7b}$$

Due to the linearity of the considered problem, we may rewrite Equation 5.7b as

$$a\left(u^{\text{S}}, \delta u^{\text{S}}\right) = (f, \delta u^{\text{S}}) - a\left(u^{\text{M}}, \delta u^{\text{S}}\right) \tag{5.8}$$

which shows readily that the coarse-scale solution u^{M} "drives" the solution of the fine-scale problem. Without additional assumptions, both Equation 5.7a and Equation 5.7b are global problems on the entire domain Ω. However, in order to reduce the computational effort, the approximation is introduced that the fine-scale problem (Equation 5.7b) if reformulated as a series of independent local problems on "patches" comprise one or more macroscale elements. In practice, these local problems are closed by, e.g., imposing homogeneous Dirichlet conditions along the patch boundary. Larson and Målqvist [17] suggest an a posteriori error estimate and an adaptive algorithm to minimize the error introduced by the boundary conditions on the patches.

We consider the discrete equivalent of Equation 5.7 in terms of nodal variables as

$$\left[\begin{array}{cc} A_{MM} & A_{MS} \\ A_{SM} & A_{SS} \end{array} \right] \left[\begin{array}{c} u_h^{\mathrm{M}} \\ u_h^{\mathrm{S}} \end{array} \right] = \left[\begin{array}{c} f^{\mathrm{M}} \\ f^{\mathrm{S}} \end{array} \right] \tag{5.9}$$

Solving for u_h^{S} from the 2nd equation in 5.9

$$u_h^{\mathrm{S}} = A_{SS}^{-1} \left(f^{\mathrm{S}} - A_{SM} u_h^{\mathrm{M}} \right) \tag{5.10}$$

and substituting u_h^{S} into the 1st equation gives the coarse scale solution u_h^{M} from

$$\left[A_{MM} - A_{MS} A_{SS}^{-1} A_{SM} \right] u_h^{\mathrm{M}} = f^{\mathrm{M}} - A_{SS}^{-1} f^{\mathrm{S}} \tag{5.11}$$

where the part $A_{MS} A_{SS}^{-1} A_{SM}$ pertains to the contribution of the fluctuation field.

Although the original purpose of VMS was to achieve stability, it has also been extensively used for coarse graining. In other words, one may use the solution on the subscale to approximate the macroscale; however, without using any homogenization. In the porous media context, Nordbotten [25] investigated a coupled Darcy flow of two phases. A similar approach was presented by Juanes [15], where the two-phase transient flow of oil and water in an oil reservoir was investigated. VMS was applied to Stokes' flow by Liu and Li in [23].

5.3 Computational Homogenization

5.3.1 Preliminaries

In order to set the stage for classical model-based homogenization, we introduce the domain decomposition $\Omega = \cup_i \Omega_{\Box,i}$, where $\Omega_{\Box,i}$ are the subdomains of predefined shape and size. We also introduce the volume averaging operator as

$$\langle f \rangle_{\Box} (\boldsymbol{x}) = \frac{1}{\mid \Omega_{\Box}(\boldsymbol{x}) \mid} \int_{\Omega_{\Box}(\boldsymbol{x})} f \mathrm{d}V \tag{5.12}$$

Setting $\Omega_{\Box}(\boldsymbol{x}) = \Omega_{\Box,i}$ when $\boldsymbol{x} \in \Omega_{\Box,i}$. This implies that $\langle f \rangle_{\Box} (\boldsymbol{x}) = \frac{1}{|\Omega_{\Box,i}|} \int_{\Omega_{\Box,i}} f \mathrm{d}V$ for $\boldsymbol{x} \in \Omega_{\Box,i}$.

As a consequence, any volume integral can be rephrased as

$$\int_{\Omega} f \mathrm{d}V = \sum_i \int_{\Omega_{\Box,i}} f \mathrm{d}V = \sum_i \int_{\Omega_{\Box,i}} \left[\frac{1}{\mid \Omega_{\Box,i} \mid} \int_{\Omega_{\Box,i}} f \mathrm{d}V' \right] \mathrm{d}V = \int_{\Omega} \langle f \rangle_{\Box} \mathrm{d}V \tag{5.13}$$

The approach taken in classical model-based homogenization is to introduce finite-sized Representative Volume Elements (RVE) such that there exist one RVE for each $\boldsymbol{x} \in \Omega$. As the RVE is of finite size, the RVEs in two sufficiently close positions will overlap. Hence,
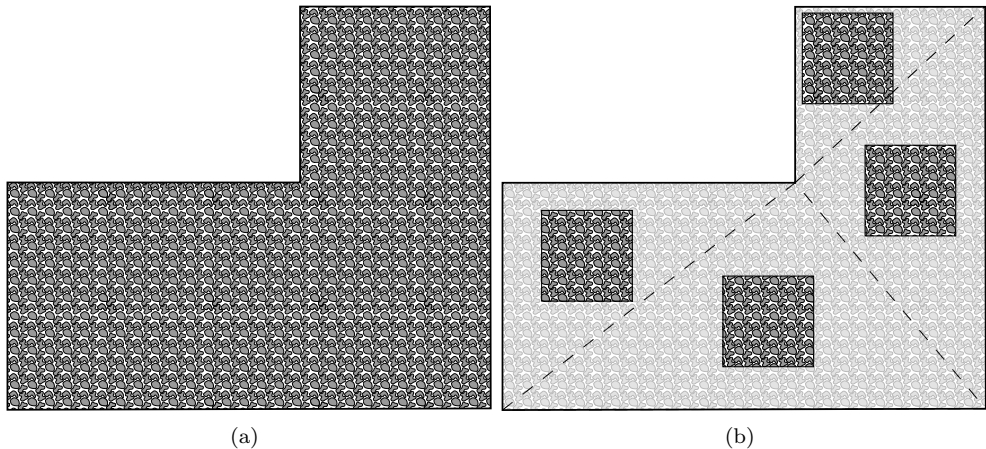
(a)   (b)

Figure 5.1: (a) Fully resolved domain (b) FE-discretization of the fully resolved domain using one Gauss-point per element where the RVE-problem is evaluated.

we introduce the approximation

$$\int_\Omega f \mathrm{d}V \approx \int_\Omega \langle f \rangle_\square \, \mathrm{d}V \tag{5.14}$$

Note that $\langle f \rangle_\square$ is smoother than f and the smoothness increases as the size of the RVE increases. Moreover, since the homogenized integral approximates the fine-scale integral, the introduced model error is expected to increase with the size unless the microsturtural features are statistically homogeneous in space (which is a common assumption in the literature of homogenization).

5.3.2   Representative Volume Element

The concept of a Representative Volume Element (RVE) was first introduced by Hill [11] and the basic idea is to use a small portion of the material to represent its macroscopic behaviour. When used in periodic structures consisting of repetitions of a simple geometry, the term "unit-cell" is often used. As an example, consider the fully resolved domain in Figure 5.1(a), consisting of two materials (dark grey and white). As the subscale geometry is very complex, performing computations directly is quite expensive. Instead we choose to conduct the analysis as shown in Figure 5.1(b)[1], where a coarse mesh is introduced. We emphasize that the geometries of the four RVEs in the figure are exactly the same.

The size of the RVE is of great importance, since a too small RVE does not capture the statistical properties of the microstructure and a too large RVE is computationally

---

[1]The example given is for illustrative purposes only. The analysis of the problem at hand would require both more elements on the domain and more than a single Gauss point per element.

inefficient. In other words, the RVE should be large enough to represent the material, i.e. an increase in size should not influence the macroscale response. It should also be large enough such that the dependence of the chosen boundary conditions of the RVE is only minor. A generally accepted requirement of scale separation is that

$$l_\mu \ll L_\square \ll L \tag{5.15}$$

where l_μ is the charateristic length of the subscale geometric features, whereas L is the typical length scale of the macroscopic domain and $L_\square$ is the characteristic length of the RVE.

For a material to be represented by an RVE, it must be statistically homogeneous, i.e. the microstructure must have the same statistical properties at two arbitrary points. There are, however, ways to handle a slowly varying microstructure, as shown in [5]. For further reading on the size of RVEs, we refer to [28].

Like in this work it is commonly assumed that an RVE is of cubic shape. This is, however, not a general requirement and other geometries have been investigated. In [9], the use of spherical RVEs is discussed; indeed, due to the lower surface to volume ratio of the sphere, it is argued that the error introduced by the boundary conditions is smaller than for the standard cube shaped RVE.

5.3.3 Homogenization - Macroscale problem

We are now in the position to replace the fine-scale potential in Equation 5.4 with the homogenized potential

$$\Pi(\hat{u}) = \int_\Omega \frac{1}{2} a_\square(\hat{u}; \hat{u}) - l_\square(\hat{u}) \, \mathrm{d}V \tag{5.16}$$

where we introduced the RVE-functional

$$a_\square(\hat{u}; \hat{v}) \stackrel{\text{def}}{=} -\langle \boldsymbol{q}(\boldsymbol{\nabla}\hat{u}) \cdot \boldsymbol{\nabla}\hat{v} \rangle_\square, \qquad\qquad l_\square(\hat{v}) \stackrel{\text{def}}{=} \langle f\hat{v} \rangle_\square \tag{5.17}$$

The stationarity condition in Equation 5.6 is now replaced by the two integrated (global) problems

$$\Pi'\left(u^{\mathrm{M}} + u^{\mathrm{S}}; \delta u^{\mathrm{M}}\right) = \int_\Omega a_\square\left(u^{\mathrm{M}} + u^{\mathrm{S}}; \delta u^{\mathrm{M}}\right) - l_\square\left(\delta u^{\mathrm{M}}\right) \mathrm{d}V = 0 \quad \forall \delta u^{\mathrm{M}} \in \mathcal{U}^{\mathrm{M},0} \tag{5.18a}$$

$$\Pi'\left(u^{\mathrm{M}} + u^{\mathrm{S}}; \delta u^{\mathrm{S}}\right) = \int_\Omega a_\square\left(u^{\mathrm{M}} + u^{\mathrm{S}}; \delta u^{\mathrm{S}}\right) - l_\square\left(\delta u^{\mathrm{S}}\right) \mathrm{d}V = 0 \qquad \forall \delta u^{\mathrm{S}} \in \mathcal{U}^{\mathrm{S}} \tag{5.18b}$$

The next step involves (i) assumption of scale separation and (ii) choice of order of homogenization. To this end, we introduce the global field $\bar{u}(\boldsymbol{x}) \in \bar{\mathcal{U}}$ for $\boldsymbol{x} \in \Omega$. We then constrain the two-scale function $u^{\mathrm{M}}(\boldsymbol{x}, \bar{\boldsymbol{x}})$ for $(\boldsymbol{x}, \bar{\boldsymbol{x}}) \in \Omega_\square(\boldsymbol{x}) \times \Omega$ pertinent to a given

RVE, via prolongation of $\bar{u}$ using 1st order Taylor series expansion within $\Omega_\square$ as follows:

$$u^{\mathrm{M}}[\bar{u}](\boldsymbol{x}, \bar{\boldsymbol{x}}) = \bar{u} + \bar{\boldsymbol{g}} \cdot [\boldsymbol{x} - \bar{\boldsymbol{x}}] \qquad \text{for } \boldsymbol{x} \in \Omega_\square \qquad (5.19)$$

where $\bar{u} \stackrel{\text{def}}{=} \bar{u}(\bar{\boldsymbol{x}})$, $\bar{\boldsymbol{g}} \stackrel{\text{def}}{=} (\boldsymbol{\nabla}\bar{u})(\bar{\boldsymbol{x}})$ and $\bar{\boldsymbol{x}}$ is, typically, defined as the "center of gravity" of the RVE, i.e. $\bar{\boldsymbol{x}} \stackrel{\text{def}}{=} \langle \boldsymbol{x} \rangle_\square$. We also for brevity, introduced the linear operator $u^{\mathrm{M}}[\bar{u}]$, which may be inserted into the RVE-integral in Equation 5.18. We consider Equation 5.18a. We obtain

$$a_\square \left(u; \delta u^{\mathrm{M}} \right) = - \langle \boldsymbol{q} \rangle_\square \cdot \delta\bar{\boldsymbol{g}} = -\bar{\boldsymbol{q}} \cdot \boldsymbol{\nabla}\delta\bar{u} \qquad (5.20)$$

$$l_\square \left(\delta u^{\mathrm{M}} \right) = \langle f \rangle_\square \, \delta\bar{u} + \langle f[\boldsymbol{x} - \bar{\boldsymbol{x}}] \rangle_\square \cdot \delta\bar{\boldsymbol{g}} = \bar{f}\delta\bar{u} + \bar{\boldsymbol{f}}^{(2)} \cdot \boldsymbol{\nabla}\delta\bar{u} \qquad (5.21)$$

where it is noted that $u = u^{\mathrm{M}}[\bar{u}] + u^{\mathrm{S}}$ and we define the macroscale quantities

$$\bar{\boldsymbol{q}} \stackrel{\text{def}}{=} \langle \boldsymbol{q} \rangle_\square, \qquad\qquad \bar{f} \stackrel{\text{def}}{=} \langle f \rangle_\square, \qquad\qquad \bar{\boldsymbol{f}}^{(2)} \stackrel{\text{def}}{=} \langle f[\boldsymbol{x} - \bar{\boldsymbol{x}}] \rangle_\square \qquad (5.22)$$

Subsequently, we ignore $\bar{\boldsymbol{f}}^{(2)}$, since it is of higher order.

The stationarity conditions in Equation 5.18 are thus replaced by the expressions

$$\Pi' \left(u^{\mathrm{M}}[\bar{u}] + u^{\mathrm{S}}; u^{\mathrm{M}}[\delta\bar{u}] \right) = \int_\Omega \left[-\bar{\boldsymbol{q}}\{\bar{u}\} \cdot \boldsymbol{\nabla}\delta\bar{u} - \bar{f}\delta\bar{u} \right] \mathrm{d}V = 0 \qquad \forall \delta\bar{u} \in \bar{\mathcal{U}}^0 \tag{5.23a}$$

$$\Pi' \left(u^{\mathrm{M}}[\bar{u}] + u^{\mathrm{S}}; \delta u^{\mathrm{S}} \right) = \int_\Omega \left[a_\square \left(u^{\mathrm{M}}[\bar{u}] + u^{\mathrm{S}}; \delta u^{\mathrm{S}} \right) - l_\square \left(\delta u^{\mathrm{S}} \right) \right] \mathrm{d}V = 0 \qquad \forall \delta u^{\mathrm{S}} \in \mathcal{U}^{\mathrm{S}} \tag{5.23b}$$

Obviously, Equation 5.23a is the homogenized (macroscale) problem, which has been obtained from Variationally Consistent Homogenization.

5.3.4 Homogenization - RVE problem

Next, we assume that it is possible to solve for u^{S} from 5.23b in an approximate manner by satisfying local problems on each RVE. Hence, we compute u^{S} on each individual RVE for any given $\bar{u} \in \bar{\mathcal{U}}$. In establishing the RVE-problems, we first note that it is only necessary to know the value of $\bar{\boldsymbol{g}}$ (and not $\bar{u}$) as input, which is inherent in computation of $\boldsymbol{q}(\boldsymbol{\nabla}u^{\mathrm{M}}[\bar{u}] + \boldsymbol{\nabla}u^{\mathrm{S}}) = \boldsymbol{q}(\bar{\boldsymbol{g}} + \boldsymbol{\nabla}u^{\mathrm{S}})$.

It is thus necessary to formulate the RVE-problems in such a manner that they are "closed", i.e. solvable, under the condition that the solution u satisfies

$$\langle \boldsymbol{\nabla}u \rangle_\square = \bar{\boldsymbol{g}} \qquad\qquad \Leftrightarrow \qquad\qquad \langle \boldsymbol{\nabla}u^{\mathrm{S}} \rangle_\square = \boldsymbol{0} \qquad (5.24)$$

This condition can be satisfied in two ways: (i) by embedding the condition (strongly) in the solution space $\mathcal{U}^{\mathrm{S}}$ for u, or (ii) by enforcing the condition in Equation 5.24 in weak

form upon introducing a Lagrange multiplier.

In conclusion, from each RVE-problem, we obtain the solution $u = u\{\bar{\boldsymbol{g}}\} = u^{\mathrm{M}}[\bar{u}] + u^{\mathrm{S}}\{\bar{\boldsymbol{g}}\}$[2]. In practice, the RVE-problems are solved in macroscale Gauss points in a nested iteration procedure between the macroscale problem (Equation 5.23a) and the RVE-problems in the FE^2 setting.

5.3.5 Macrohomogeneity condition

Let us introduce the residuals

$$R(u, \delta u) \overset{\mathrm{def}}{=} \Pi'(u; \delta u) \tag{5.25}$$

$$\bar{R}\{\bar{u}, \delta\bar{u}\} \overset{\mathrm{def}}{=} \Pi'\left(u^{\mathrm{M}}[\bar{u}] + u^{\mathrm{S}}\{\bar{u}\}; u^{\mathrm{M}}[\delta\bar{u}]\right) \tag{5.26}$$

whereby it follows that the macroscale problem can be rephrased as: Find $\bar{u} \in \bar{\mathcal{U}}$ such that

$$\bar{R}\{\bar{u}, \delta\bar{u}\} = 0 \qquad\qquad \forall\delta\bar{u} \in \bar{\mathcal{U}}^0 \tag{5.27}$$

Moreover, we introduce the macroscale potential

$$\bar{\Pi}\{\bar{u}\} \overset{\mathrm{def}}{=} \Pi\left(u^{\mathrm{M}}[\bar{u}] + u^{\mathrm{S}}\{\bar{u}\}\right) \tag{5.28}$$

whose stationary point is defined by

$$\begin{aligned}
\bar{\Pi}'\{\bar{u}; \delta\bar{u}\} = \Pi'\left(u^{\mathrm{M}}[\bar{u}] + u^{\mathrm{S}}\{\bar{u}\}; u^{\mathrm{M}}[\delta\bar{u}] + (u^{\mathrm{S}})'\{\bar{u}; \delta\bar{u}\}\right) = \\
\bar{R}\{\bar{u}, \delta\bar{u}\} + \Pi'\left(u^{\mathrm{M}}[\bar{u}] + u^{\mathrm{S}}\{\bar{u}\}; (u^{\mathrm{S}})'\{\bar{u}; \delta\bar{u}\}\right) = 0 \quad (5.29)
\end{aligned}$$

where $\mathrm{d}u^{\mathrm{S}} \overset{\mathrm{def}}{=} (u^{\mathrm{S}})'\{\bar{u}; \mathrm{d}\bar{u}\}$ is the sensitivity of u^{S} for a change of the macroscale field $\bar{u}$.

We should now require that

$$\bar{\Pi}'\{\bar{u}; \delta\bar{u}\} = \bar{R}\{\bar{u}, \delta\bar{u}\} = 0 \tag{5.30}$$

i.e. that the solution $\bar{u}$ to the residual equation 5.27 is the same as the stationary point defined by 5.29. The condition is obviously that

$$\Pi'\left(u\{\bar{u}\}; (u^{\mathrm{S}})'\{\bar{u}; \delta\bar{u}\}\right) = 0 \qquad\qquad \forall\delta\bar{u} \in \bar{\mathcal{U}}^0 \tag{5.31}$$

where $u\{\bar{u}\} = u^{\mathrm{M}}[\bar{u}] + u^{\mathrm{S}}\{\bar{u}\}$. We may localize this condition to an individual RVE as

$$a_\square\left(u\{\bar{u}\}; (u^{\mathrm{S}})'\{\bar{u}; \delta\bar{u}\}\right) - l_\square\left((u^{\mathrm{S}})'\{\bar{u}; \delta\bar{u}\}\right) = 0 \qquad\qquad \forall\delta\bar{u} \in \bar{\mathcal{U}}^0 \tag{5.32}$$

---

[2]Curly brackets $\{\bullet\}$ indicates implicit function of the arguments

or, more explicitly

$$-\left\langle \boldsymbol{q} \cdot \boldsymbol{\nabla} \mathrm{d}u^{\mathrm{S}} \right\rangle_{\square} - \left\langle f \mathrm{d}u^{\mathrm{S}} \right\rangle_{\square} = 0 \qquad\qquad \forall \mathrm{d}\bar{u} \in \bar{\mathcal{U}}^0 \qquad (5.33)$$

where we used the abbreviated notation $\boldsymbol{q} = \boldsymbol{q}(\boldsymbol{\nabla} u\{\bar{u}\})$ and $\mathrm{d}u^{\mathrm{S}} = (u^{\mathrm{S}})'\{\bar{u}; \mathrm{d}\bar{u}\}$ is a sensitivity w.r.t. a change of $\bar{u}$. Upon integrating by parts in the first term in Equation 5.33, we obtain the alternative formulation, with $q_n \stackrel{\mathrm{def}}{=} \boldsymbol{q} \cdot \boldsymbol{n}$,

$$\int_{\Gamma_{\square}} q_n \mathrm{d}u^{\mathrm{S}} \mathrm{d}S = 0 \qquad\qquad (5.34)$$

Equations 5.33 and 5.34 are alternative formulations of a local macrohomogeneity condition. Its relation to the classical Hill-Mandel condition is discussed next.

To simplify the discussion, assume that f is smooth such that $\left\langle f \mathrm{d}u^{\mathrm{S}} \right\rangle_{\square} \approx \bar{f} \left\langle \mathrm{d}u^{\mathrm{S}} \right\rangle_{\square} = 0$ (since $\left\langle u^{\mathrm{S}} \right\rangle_{\square} = 0$). Now, insert this assumption in Equation 5.33 and consider

$$\langle \boldsymbol{q} \cdot \boldsymbol{\nabla} \mathrm{d}u \rangle_{\square} = \langle \boldsymbol{q} \rangle_{\square} \cdot \underbrace{\mathrm{d}\bar{\boldsymbol{g}}}_{=\langle \boldsymbol{\nabla} \mathrm{d}u \rangle_{\square}} + \underbrace{\langle \boldsymbol{q} \cdot \boldsymbol{\nabla} \mathrm{d}u^{\mathrm{S}} \rangle_{\square}}_{=0} = \langle \boldsymbol{q} \rangle_{\square} \cdot \langle \boldsymbol{\nabla} \mathrm{d}u \rangle_{\square} \qquad (5.35)$$

where $\mathrm{d}u = \mathrm{d}u\{\bar{u}; \mathrm{d}\bar{u}\}$, is the sensitivity of u w.r.t. a change $\mathrm{d}\bar{u} \in \bar{\mathcal{U}}^0$. Clearly, the condition bears a strong resemblance with the classic Hill-Mandel condition, which reads

$$\langle \boldsymbol{q} \cdot \boldsymbol{\nabla} u \rangle_{\square} = \langle \boldsymbol{q} \rangle_{\square} \cdot \langle \boldsymbol{\nabla} u \rangle_{\square} \qquad\qquad (5.36)$$

where $u = u\{\bar{u}\}$ is the actual solution of the RVE problem.

Finally, we may interpret the derivation above in terms of the diagram in Figure 5.2. Departing from the potential $\Pi(u)$ in the left upper corner, we may arrive at the result $\Pi'\left(u^{\mathrm{M}} + u^{\mathrm{S}}; \delta u^{\mathrm{M}}\right) = 0$ in the lower right corner in two ways: (i) Establish the stationarity condition $\Pi'(u; \delta u^{\mathrm{M}}) = 0$ (left vertical arrow) and introduce the split $u = u^{\mathrm{M}} + u^{\mathrm{S}}\{u^{\mathrm{M}}\}$ or, (ii) Establish $\Pi\left(u^{\mathrm{M}} + u^{\mathrm{S}}\{u^{\mathrm{M}}\}\right)$ and carry out the variation w.r.t. u^{M}, while also using the macrohomogeneity condition (right vertical arrows).

In [18], VCH is used to handle the problem of uncoupled consolidation and is later extended in [36] where the coupled case is presented. Larsson et al [21] employs VCH to study a non-linear transient heat flow problem. Nilenius et al [24] studies diffusion of moisture and chloride ion in concrete using VCH. Öhman et al [27] uses VCH for simulating sintering. Here, the subscale consists of Tungsten-Carbide solid particles in a Cobolt liquid binder. Although each constituent is incompressible, the material is considered as compressible on the macroscale due to shrinking porosity.

Finally, it should be noted that VCH does not inherently adopt the assumption of scale-separation. It is thus possible to seamlessly use homogenization in only parts of a domain, cf. [19][20].
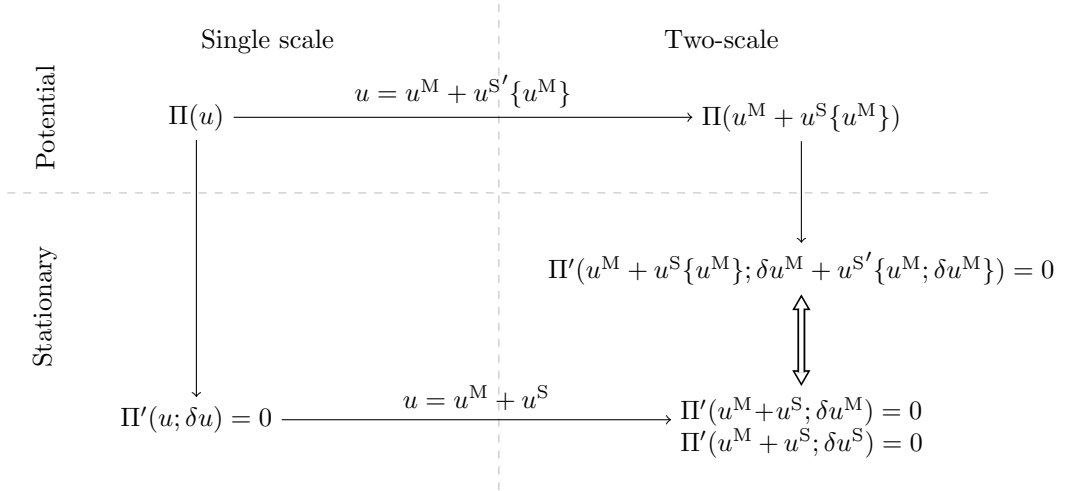
Single scale   **Two-scale**

Potential

$\Pi(u) \xrightarrow{\quad u = u^{\mathrm{M}} + u^{\mathrm{S}'}\{u^{\mathrm{M}}\}\quad} \Pi(u^{\mathrm{M}} + u^{\mathrm{S}}\{u^{\mathrm{M}}\})$

Stationary

$\Pi'(u^{\mathrm{M}} + u^{\mathrm{S}}\{u^{\mathrm{M}}\}; \delta u^{\mathrm{M}} + u^{\mathrm{S}'}\{u^{\mathrm{M}}; \delta u^{\mathrm{M}}\}) = 0$

$\Pi'(u; \delta u) = 0 \xrightarrow{\quad u = u^{\mathrm{M}} + u^{\mathrm{S}}\quad} \begin{matrix}\Pi'(u^{\mathrm{M}} + u^{\mathrm{S}}; \delta u^{\mathrm{M}}) = 0 \\ \Pi'(u^{\mathrm{M}} + u^{\mathrm{S}}; \delta u^{\mathrm{S}}) = 0\end{matrix}$

Figure 5.2: The figure shows two different ways of deriving the macroscale problem from an underlying finescale potential, either by first introducing the stationarity condition and subsequently the two-scale ansatz, or vice-versa. Identical results are obtained if the macrohomogeneity condition, illustrated by the double arrow, is fulfilled

6 Summary of appended papers

6.1 Paper A: Variationally Consistent Homogenization of Stokes Flow in Porous Media

A possibly non-linear fluid is present in a rigid skeleton. Using variationally consistent homogenization, a two-scale problem consisting of a Darcy flow on the macroscale and a Stokes flow on the subscale is derived. The subscale pressure and velocity fields are treated as implicitly dependent on the macroscale pressure. Prolongation conditions linking the macroscale and the subscale is introduced such that the macroscale pressure gradient and the average subscale pressure gradient is equivalent. It is shown that the periodic boundary condition satisfies the Variationally Consistent Macrohomogeneity Condition.

Two 2D numerical examples are given. The first concerns the permeability of RVEs containing circular obstacles. Obstacles of different patterns are considered as well as the size of the RVE. The second concerns the macroscopic effect of the non-linear fluid on the subscale.

6.2 Paper B: A Two-scale Finite Element Formulation of Stokes Flow in Porous Media

An iterative FE^2 method is devised where the subscale problem is used as a constitutive model. The subscale sensitivity pertinent to the macroscale tangent problem is discussed for both linear an non-linear flows. On the RVE, periodic boundary conditions are used.

Two 2D examples are given. The first pertains to the evaluation of the macroscale difference between a linear and a non-linear fluid being present on the subscale. The second example aims at evaluating the difference of a fully resolved problem to a the solution of a fully concurrent multiscale problem.

6.3 Paper C: Weakly Periodic Boundary Conditions for the Homogenization of Flow in Porous Media

From the energy potential on a fully resolved domain, the two-scale problem is derived such that an optimization (saddle-point) problem exists on both scales. It is shown that the weak form of the problem is the same as that presented in Paper A. The concept of weakly periodic boundary conditions for Stokes flow is introduced such that we can impose periodicity on a non-periodic computational grid with periodic geometry. As a result, unknown terms relevant to the required traction and flux along the boundary arise. Upper and lower bounds for the energy in the strongly periodic solution is discussed. It is shown how imposing strongly periodic velocity or pressure fields on a non-periodic mesh in 2D, results in energetic bounds. It is also shown that in the special case of linear flow, the upper and lower bounds of the permeability can be computed.

Two 2D examples are shown. In the first, the effect of Weakly Periodic Boundary Conditions using global polynomials of varying degree as approximations of the unknown tractions and fluxes is investigated. The second example discuss the impact of RVE size on the permeability using the Weakly Periodic Boundary Condition.

6.4 Paper D: On Bounded Approximations of Periodicity for Computational Homogenization of Stokes Flow in Porous Media

In this paper, we derive the two-scale problem from a potential on a fully resolved domain. A proposal on how to evaluate the upper and lower energy bounds for the strongly periodic case, using a special type of shape functions for the velocity and pressure fields is given. As prescribing the shape of the flow periodically on a non-periodic mesh can introduce artificial compressibility in the model, correction factors corresponding to the shape functions are derived. The shape functions are constructed from snap-shots on

the boundary of pre-computed approximations and are termed Solution Based Shape Functions.

Two numerical 3D examples are given. In the first, upper and lower bounds for the permeability of the strongly periodic case is computed along with the permeability for the weakly periodic solution. In the second example, we investigate the Solution Based Shape Functions stemming from weakly periodic solutions of different approximation.

6.5 Paper E: Homogenization of Coupled Flow and Deformation in a Porous Material

The main focus of this paper is the interaction between an elastic solid skeleton and the fluid contained within. Starting from two separate problems, one pertinent to the FSI problem and one pertinent to the deformation of the computational mesh in the fluid part of the domain, a monolithic FSI formulation is produced. Special attention is given to the apparatus handling the deformation of the computational mesh such that no additional stiffness is introduced. Using the devised model, the Biot coefficient can be computed.

Two 3D examples are given. In the first example, we investigate how the Biot coefficient changes with a prescribed total pressure in the RVE with various choices of bulk modulus. The second example discuss how the seepage varies with different deformation modes of different magnitude.

7   Thesis outcome

- In Paper A, a possibly non-linear Stokes flow is homogenized using the Variationally Consistent Homogenization framework. As an extension, the fully concurrent setting is introduced in Paper B. Numerical investigations shows that the results of the homogenized problem correlates well with the results of the fully resolved problem.

- To deal with the problem of periodic boundary conditions on an arbitrary mesh, we introduce the concept of Weak Periodic Boundary Conditions in 2D for a Stokes flow in Paper C. In Paper D, the Weak Periodic Boundary Condition is extended to 3D.

- In order to evaluate the performance of the Weak Periodic Boundary Conditions, we show how to compute the upper and lower energy bounds in Paper C for 2D. For the same bounds to be computed in 3D, we introduce the concept of Solution Based Shape Functions in Paper D.

- In Paper E, we introduce a fictitious elastic material in order to cope with the problem of invalid discretization on the fluid domain in an FSI formulation. The result is a monolithic FSI method with an incorporated mesh smoothing procedure.

- In Paper E it is shown how the Biot coefficient can be computed numerically in the limit of small deformations, i.e. for a linearized model.

8 Conclusions and future work

In this thesis, a first order homogenization scheme pertinent to a Stokes flow on the subscale and a Darcy flow on the macroscale is presented. The two-scale formulation is derived using the Variationally Consistent Homogenization method such that the derivation start out from the fully resolved problem. A formulation for the case of flow in deformable porous media is also presented. In the latter, the momentum balance equation for the solid phase is also present on both scales.

It is shown that the boundary conditions used in the examples fulfills the Variationally Consistent Macrohomogeneity Condition, thus, we ensure that no artificial energy source or sink is present in the model. The boundary conditions used on the RVE are periodic boundary conditions for the fluid and Dirichlet boundary conditions on the solid when present.

In the context of phenomenological modeling of porous materials, a great number of parameters concerning processes such as erosion, consolidation and sedimentation has to be calibrated. This is a difficult and often expensive task due to the need of experimental data. Thus, a natural extension of this research is to include these processes.

For very large deformations of porous materials the walls of the solid phase inside the material will be subject to contact. Therefore, the impact of internal contact should be evaluated.

A large number of applications, such as simulation of oil reservoirs, calls for the ability to handle two or more fluid phases. This includes the simulation of non-saturated porous material. This also implies that capillary forces has to be taken into consideration.

When evaluating solid materials, Dirichlet and Neumann boundary conditions pertains to the upper and lower bounds of the samples stiffness. Here, the Dirichlet and Neumann boundary conditions pertains to the upper and lower bounds for the permeability. Some problems arise with these conditions, for example, we cannot ensure global incompressibility for the Dirichlet boundary conditions unless special care are taken concerning the velocity profile. In order to evaluate the said bounds, this matter should be attended.

Due to the high computational cost involved in a fully concurrent multiscale analysis, an investigation in suitable macroscopic phenomenological models, capable of capturing the properties on the subscale should be executed. One alternative approach is to use a sufficiently good phenomenological model to find a good initial guess for the fully concurrent problem. Another suggestion is to employ some method of model reduction (mode decomposition) such as Eigendecomposition or Proper Generalized Decomposition.

References

[1] M. A. Biot. Theory of Elasticity and Consolidation for a Porous Anisotropic Solid. *Journal of Applied Physics* **26**.2 (1955), 182. ISSN: 00218979. DOI: 10.1063/1.1721956. URL: http://scitation.aip.org/content/aip/journal/jap/26/2/10.1063/1.1721956.

[2] M. a. Biot. Mechanics of Deformation and Acoustic Propagation in Porous Media. *Journal of Applied Physics* **33**.4 (1962), 1482. ISSN: 00218979. DOI: 10.1063/1.1728759. URL: http://scitation.aip.org/content/aip/journal/jap/33/4/10.1063/1.1728759.

[3] M. A. Biot. General Theory of Three-Dimensional Consolidation. *Journal of Applied Physics* **12**.2 (1941), 155. ISSN: 00218979. DOI: 10.1063/1.1712886. URL: http://scitation.aip.org/content/aip/journal/jap/12/2/10.1063/1.1712886.

[4] F. Brezzi et al. *Stabilization techniques and subgrid scales capturing*. 1996, pp. 1–17. URL: http://math.ucdenver.edu/ccm/reports/rep083.pdf.

[5] D. L. Brown, P. Popov, and Y. Efendiev. On homogenization of stokes flow in slowly varying media with applications to fluid–structure interaction. *GEM - International Journal on Geomathematics* **2**.2 (Sept. 2011), 281–305. ISSN: 1869-2672. DOI: 10.1007/s13137-011-0025-y. URL: http://link.springer.com/10.1007/s13137-011-0025-y.

[6] H. Darcy. *Les Fontaines Publiques de la Ville de Dijon*. 1856.

[7] L. J. Gibson. Biomechanics of cellular solids. *Journal of biomechanics* **38**.3 (Mar. 2005), 377–99. ISSN: 0021-9290. DOI: 10.1016/j.jbiomech.2004.09.027. URL: http://www.ncbi.nlm.nih.gov/pubmed/15652536.

[8] GlassFiberStore. *Glass Fiber Store*. 2015. URL: http://www.glassfiberstore.com/glass-fiber-filters/advantec-mfs/gc50-glass-fiber.html.

[9] R. Glüge, M. Weber, and A. Bertram. Comparison of spherical and cubical statistical volume elements with respect to convergence, anisotropy, and localization behavior. *Computational Materials Science* **63** (Oct. 2012), 91–104. ISSN: 09270256. DOI: 10.1016/j.commatsci.2012.05.063. URL: http://linkinghub.elsevier.com/retrieve/pii/S0927025612003448.

[10] M. Heil, A. L. Hazel, and J. Boyle. Solvers for large-displacement fluid–structure interaction problems: segregated versus monolithic approaches. *Computational Mechanics* **43**.1 (Mar. 2008), 91–101. ISSN: 0178-7675. DOI: 10.1007/s00466-008-0270-6. URL: http://link.springer.com/10.1007/s00466-008-0270-6.

[11] R. Hill. Elastic properties of reinforced solids: some theoretical principles. *Journal of the Mechanics and Physics of Solids* **I**.Hill 1962 (1963). URL: http://www.sciencedirect.com/science/article/pii/002250966390036X.

[12] G. Hou, J. Wang, and A. Layton. Numerical Methods for Fluid-Structure Interaction - A Review. *Communications in Computational Physics* **12**.2 (2012), 337–377. ISSN: 18152406. DOI: 10.4208/cicp.291210.290411s. URL: http://www.global-sci.com/issue/abstract/readabs.php?vol=12%5C&page=337%5C&issue=2%5C&ppage=377%5C&year=2012.

[13] T. Hughes. Multiscale phenomena: Green's functions, the Dirichlet-to-Neumann formulation, subgrid scale models, bubbles and the origins of stabilized methods. *Computer methods in applied mechanics and . . .* **7825** (1995). URL: http://www.sciencedirect.com/science/article/pii/0045782595008449.

[14] O. Iliev, A. Mikelic, and P. Popov. On upscaling certain flows in deformable porous media. *Multiscale Modeling & Simulation* **7**.1 (2008), 93–123. URL: http://epubs.siam.org/doi/abs/10.1137/06067732X.

[15] R. Juanes. A variational multiscale finite element method for multiphase flow in porous media. *Finite Elements in Analysis and Design* **41**.7-8 (Apr. 2005), 763–777. ISSN: 0168874X. DOI: 10.1016/j.finel.2004.10.008. URL: http://linkinghub.elsevier.com/retrieve/pii/S0168874X04001714.

[16] S. Kim and S. J. Karrila. *Microhydrodynamics.* Elsevier, 1991, pp. 1–12. ISBN: 9780750691734. DOI: 10.1016/B978-0-7506-9173-4.50007-4. URL: http://www.sciencedirect.com/science/article/pii/B9780750691734500074.

[17] M. G. Larson and A. Målqvist. Adaptive variational multiscale methods based on a posteriori error estimation: Energy norm estimates for elliptic problems. *Computer Methods in Applied Mechanics and Engineering* **196**.21-24 (Apr. 2007), 2313–2324. ISSN: 00457825. DOI: 10.1016/j.cma.2006.08.019. URL: http://linkinghub.elsevier.com/retrieve/pii/S0045782506003902.

[18] F. Larsson, K. Runesson, and F. Su. Computational homogenization of uncoupled consolidation in micro-heterogeneous porous media. *International Journal for Numerical and Analytical Methods in Geomechanics* **34**.14 (2010), 1431–1458. ISSN: 03639061. DOI: 10.1002/nag.862. URL: http://onlinelibrary.wiley.com/doi/10.1002/nag.862/full.

[19] F. Larsson and K. Runesson. Adaptive Bridging of Scales in Continuum Modeling Based on Error Control. *International Journal for Multiscale Computational Engineering* **6**.4 (2008), 371–392. ISSN: 15431649. DOI: 10.1615/IntJMultCompEng.v6.i4.80. URL: http://www.begellhouse.com/journals/61fd1b191cf7e96f,6a4cc29505086840,7cf86741344095e8.html.

[20] F. Larsson and K. Runesson. On two-scale adaptive FE analysis of micro-heterogeneous media with seamless scale-bridging. *Computer Methods in Applied Mechanics and Engineering* **200**.37-40 (Sept. 2011), 2662–2674. ISSN: 00457825. DOI: 10.1016/j.cma.2010.10.012. URL: http://linkinghub.elsevier.com/retrieve/pii/S0045782510002902.

[21] F. Larsson, K. Runesson, and F. Su. Variationally consistent computational homogenization of transient heat flow. *International Journal for Numerical Methods in Engineering* **81**.13 (2009), 1659–1686.

[22] B. Lenhof, F. Larsson, and K. Runesson. A comparison of variational formats for porous media subjected to dynamic loading. *International Journal for . . .* April 2010 (2011), 807–823. DOI: 10.1002/nag. URL: http://onlinelibrary.wiley.com/doi/10.1002/nag.925/full.

[23] X. Liu and S. Li. A variational multiscale stabilized finite element method for the Stokes flow problem. *Finite Elements in Analysis and Design* **42**.7 (Apr. 2006), 580–591. ISSN: 0168874X. DOI: 10.1016/j.finel.2005.11.006. URL: http://linkinghub.elsevier.com/retrieve/pii/S0168874X05001526.

[24] F. Nilenius and F. Larsson. Macroscopic diffusivity in concrete determined by computational homogenization. *International Journal for Numerical and Analytical Methods in Geomechanics* May 2012 (2012), 1535–1551. DOI: `10.1002/nag`. URL: `http://onlinelibrary.wiley.com/doi/10.1002/nag.2097/full`.

[25] J. Nordbotten. Adaptive variational multiscale methods for multiphase flow in porous media. *Multiscale Modeling & Simulation* **7**.3 (2009), 1455–1473. URL: `http://epubs.siam.org/doi/abs/10.1137/080724745`.

[26] N. Nowak, P. P. Kakade, and A. V. Annapragada. Computational Fluid Dynamics Simulation of Airflow and Aerosol Deposition in Human Lungs. *Annals of Biomedical Engineering* **31**.4 (Apr. 2003), 374–390. ISSN: 0090-6964. DOI: `10.1114/1.1560632`. URL: `http://link.springer.com/10.1114/1.1560632`.

[27] M. Ohman, K. Runesson, and F. Larsson. Computational Mesoscale modeling and homogenization of liquid-phase sintering of particle agglomerates. *Technische Mechanik* **32** (2011), 463–483. URL: `http://www.ovgu.de/ifme/zeitschrift%5C_tm/2012%5C_Heft2%5C_5/33%5C_Oehman.pdf`.

[28] M. Ostoja-Starzewski. Material spatial randomness: From statistical to representative volume element. *Probabilistic Engineering Mechanics* **21**.2 (Apr. 2006), 112–132. ISSN: 02668920. DOI: `10.1016/j.probengmech.2005.07.007`. URL: `http://linkinghub.elsevier.com/retrieve/pii/S0266892005000433`.

[29] E. Sánchez-Palencia. *Non-homogeneous media and vibration theory.* Springer-Verlag, 1980. ISBN: 3-540-10000-8.

[30] C. Sandström and F. Larsson. On Bounded Approximations of Periodicity for Computational Homogenization of Stokes Flow in Porous Media. *Submitted for international publication* ().

[31] C. Sandström and F. Larsson. Variationally Consistent Homogenization of Stokes Flow in Porous Media. *International Journal for Multiscale Computational Engineering* **11**.2 (2013), 117–138. ISSN: 1543-1649. DOI: `10.1615/IntJMultCompEng.2012004069`. URL: `http://www.begellhouse.com/journals/61fd1b191cf7e96f,6218a4594d64a04c,4e77728141fddda9.html`.

[32] C. Sandström, F. Larsson, and K. Runesson. Homogenization of Coupled Flow and Deformation in a Porous Material. *To be submitted* ().

[33] C. Sandström, F. Larsson, and K. Runesson. Weakly Periodic Boundary Conditions for the Homogenization of Flow in Porous Media. *Advanced Modeling and Simulation in Engineering Sciences* **1**.1 (2014), 12. ISSN: 2213-7467. DOI: `10.1186/s40323-014-0012-6`. URL: `http://www.amses-journal.com/content/1/1/12`.

[34] C. Sandström et al. A Two-scale Finite Element Formulation of Stokes Flow in Porous Media. *Computer Methods in Applied Mechanics and Engineering* **261-262** (July 2013), 96–104. ISSN: 00457825. DOI: `10.1016/j.cma.2013.03.025`. URL: `http://linkinghub.elsevier.com/retrieve/pii/S0045782513000856`.

[35] B. Soni and S. Aliabadi. Large-scale CFD simulations of airflow and particle deposition in lung airway. *Computers & Fluids* **88** (Dec. 2013), 804–812. ISSN: 00457930. DOI: `10.1016/j.compfluid.2013.06.015`. URL: `http://linkinghub.elsevier.com/retrieve/pii/S0045793013002387`.

[36] F. Su, F. Larsson, and K. Runesson. Computational homogenization of coupled consolidation problems in micro-heterogeneous porous media. *International Journal*

for ... June (2011), 1198–1218. DOI: 10.1002/nme. URL: http://onlinelibrary.
wiley.com/doi/10.1002/nme.3221/full.

[37]   University of Strathclyde. *University of Strathclyde.* URL: https://www.strath.ac.
uk/civeng/research/geomechanics/.

[38]   Wikipedia. *Wikipedia.* 2015. URL: http://en.wikipedia.org/wiki/Soil.